

## The effect of Fullerene (C<sub>60</sub>) nanoparticles on the surface of PVDF composite membrane

Kyung Hee Kim<sup>1</sup>, Ju Sung Lee<sup>1</sup>, Hyun Pyo Hong<sup>1</sup>,  
Jun Young Han<sup>2</sup>, Jin-Won Park<sup>1</sup> and ByoungRyul Min<sup>\*1</sup>

<sup>1</sup> Department of Chemical and Biomolecular Engineering, Yonsei University,  
262 Seongsanno, Seodaemun-gu, Seoul 120-749, South Korea

<sup>2</sup> Fuel Cell Research Center, Korea Institute of Science and Technology,  
39-1 Hawolgok-dong, Sungbuk-gu, Seoul 136-791, Republic of Korea

(Received July 10, 2014, Revised July 07, 2015, Accepted August 24, 2015)

**Abstract.** Polyvinylidene fluoride/fullerene nanoparticle (PVDF/C<sub>60</sub>) composite microfiltration (MF) membranes were fabricated by a non-solvent induced phase separation (NIPS) using N, N-dimethylacetamide (DMAc) as solvent and deionized water (DI) as coagulation solution. Polyvinylpyrrolidone (PVP) was added to the casting solution to form membrane pores. C<sub>60</sub> was added in increments of 0.2% from 0.0% to 1.0% to produce six different membrane types: one pristine PVDF membrane type with no C<sub>60</sub> added as control, and five composite membrane types with varying C<sub>60</sub> concentrations of 0.2, 0.4, 0.6, 0.8 and 1.0%, respectively. The mechanical strength, morphology, pore size and distribution, hydrophilicity, surface property, permeation performance, and fouling resistance of the six membranes types were characterized using respective analytical methods. The results indicate that membranes containing C<sub>60</sub> have higher surface porosity and pore density than the pristine membrane. The presence of numerous pores on the membrane caused weaker mechanical strength, but the water flux of the composite membranes increased in spite of their smaller size. Initial flux and surface roughness reached the maximum point among the composite membranes when the C<sub>60</sub> concentration was 0.6 wt.%.

**Keywords:** polyvinylidene fluoride (PVDF); fullerene (C<sub>60</sub>); phase inversion; microfiltration (MF); composite membrane

### 1. Introduction

Numerous attempts have been made over the last several decades to develop new composite materials to improve both chemical and mechanical properties of microfiltration (MF) membranes (Wu *et al.* 2008). The general purpose of such studies is to achieve uniform pore formation, and to increase flux, permeability, and removal rate. Improvement in refreshment rates and reduction of fouling are also economic goals in attempting to improve the value of the material (Rana and Matsuura 2010, Yang *et al.* 2010).

PVDF is a superior material with excellent chemical resistance and mechanical properties, and has been noted as an excellent material in the field of membrane separation due to its convenient

---

\*Corresponding author, Professor, E-mail: [minbr345@yonsei.ac.kr](mailto:minbr345@yonsei.ac.kr)

solubility characteristics (Bottino *et al.* 2005, Chae *et al.* 2008, Madaeni and Yeganeh 2003, Oshima *et al.* 1996, Park *et al.* 2007, Tan *et al.* 2006, Wang *et al.* 2004). Research for water treatment applications of PVDF has been conducted in various fields, including improvement of performance through fouling reduction and addition of non-organic particles. However, in the field of water treatment, hydrophobic properties have caused deterioration of flux and membrane fouling; as a result, many researchers have attempted to enhance the hydrophilicity of PVDF membranes through various modifications such as polymer blending, synthesis of hydrophilic functional groups, and addition of diverse particles. Zhang (Zhang *et al.* 2009) reported on hydrophilic modification of PVDF MF membrane by blending of polyethersulfone (PES). Ochoa (Ochoa *et al.* 2003) investigated polyvinylidene fluoride/polymethyl methacrylate (PVDF/PMMA) blend membrane, which has a lower contact angle than pure PVDF membrane. Wang (Wang *et al.* 2002) immobilized and grafted polyethylene glycol (PEG) onto the PVDF MF membrane surface to improve its antifouling properties. Preparation of nanomaterial-doped membranes is another innovative way to improve membrane properties. There are some notable studies on materials with such characteristics, involving inorganic materials such as TiO<sub>2</sub> (Bae and Tak 2005, Cao *et al.* 2006, Oh *et al.* 2009, Rahimpour *et al.* 2011), Al<sub>2</sub>O<sub>3</sub> (Yan *et al.* 2006), and ZrO<sub>2</sub> (Zheng *et al.* 2011).

Porous carbon-based substances have also been noted recently, and although their characteristics are different from the aforementioned inorganic additive particles, they have also been used as additives for membranes. Vatanpour (Vatanpour *et al.* 2011) reported on the effect of multi-walled carbon nanotubes (MWCNTs) as additive in terms of compatibility with polymers, along with their influence on pore size and porosity. Spherical fullerene (C<sub>60</sub>), which is also referred to as a buckyball, is another carbon-based nanoparticle which may be used as additive to achieve limited increase in hydrophilicity and flux (Arthanareeswaran *et al.* 2008, Taurozzi *et al.* 2011). Ma (Ma *et al.* 2010) investigated its particle behavior in aqueous systems. Ironically, the strong condensation of water induces C<sub>60</sub> aggregation when it is immersed in water, but in polymer structure, it remains well-dispersed, indicating extraordinary behavior.

This study looks at the structural characteristics of MF membranes produced with varying compositions of PVDF/C<sub>60</sub> blending solutions, and the effect of C<sub>60</sub> on water treatment performance. In order to assess such effect, the fabricated composite membranes were analyzed for tensile strength (kPa) and elongation (%) at break, surface and cross-section morphologies, pore size and distribution, surface porosity and pore density, water contact angle, surface roughness, flux, rejection, and fouling, in comparison with pristine PVDF membranes.

## 2. Experimental

### 2.1 Materials

The membrane-forming polymer polyvinylidene fluoride (PVDF), Solef<sup>®</sup> 1015 (MW = 573,000 g/mol), was provided by Solvay Korea Co., Korea. The solvent for membrane fabrication, N, N-dimethylacetamide (DMAc), was purchased from Sigma Aldrich, USA. The fullerene nanoparticles (C<sub>60</sub> 98%, MW = 720.64 g/mol) were also purchased from Sigma Aldrich. The additive to form pores in membranes, polyvinylpyrrolidone (PVP, K = 15), was obtained from TCI, Japan. Kaolin for particle rejection and humic acid for fouling test were provided from Sigma Aldrich.

Table 1 Composition of dope solutions

Solution	PVDF (wt.%)	PVP (wt.%)	$C_{60}$ (wt.%)	DMAc (wt.%)	$C_{60}$ /PVDF (%)
$C_{60}$ -0	13	10	0	77	0.0
$C_{60}$ -1	13	10	0.026	76.974	0.2
$C_{60}$ -2	13	10	0.052	76.948	0.4
$C_{60}$ -3	13	10	0.078	76.922	0.6
$C_{60}$ -4	13	10	0.104	76.896	0.8
$C_{60}$ -5	13	10	0.130	76.870	1.0

## 2.2 Fabrication of membranes

Dry fullerene powder was suspended in DMAc and sonicated for 2 h to produce fullerene/DMAc organosol. PVDF and PVP were dissolved in organosol mixture for 24 h at 60°C under continuous stirring to obtain a homogenous solution. The composition of dope solution is listed in Table 1. Membranes were fabricated by a non-solvent induced phase inversion method, and the entire process was carried out at room temperature. After cooling down the solution at room temperature, the solution was then cast on polyester non-woven fabric using a 200  $\mu$ m-height-casting-knife. Afterwards, a thin non-woven fabric film was immersed in DI water coagulation bath for 24 h to remove the remaining solvent. The membranes were dried at 25°C for 24 h.

## 2.3 Characterization of membranes

### 2.3.1 Tensile strength and elongation at break

The tensile strength (kPa) and elongation (%) at break of the membranes were measured using a universal testing machine (UTM, Multi test 1-I, Mecmesin, United Kingdom). Rectangular samples (30 mm  $\times$  10 mm) were prepared from each membrane and measured with a gauge length of 20 mm at stretching speed of 50 mm/min. All experiments were carried out at room temperature.

### 2.3.2 Structure of membrane surfaces and cross-sections

Surface and cross-section structures were observed using a field emission scanning electron microscope (FE-SEM, JEOL-6701F, JEOL, Japan). Supportless membranes were especially manufactured to verify cross-section. Samples for cross-sections were dipped frozen in liquid nitrogen and then fractured. All surfaces and cross-sections were coated with platinum (Pt). At the same time, energy dispersive X-ray spectroscopy (EDS, Oxford, JEOL) was used to analyze presence of fullerene nanoparticles on membrane surfaces.

### 2.3.3 Properties of pores

The properties of pores on each membrane were investigated with a capillary flow porometer (CFP-1200-AEL, Porous Materials, Inc., USA) using a statistic method. The capillary flow porometer was used to determine the average pore radii and pore distribution. Samples were put in Galwick (15.9 dynes/cm) for 24 h to fill membrane pores completely with wetting liquid. The liquid was displaced by increasing nitrogen gas pressure. Mean flow pore diameter, bubble point pore diameter, and pore size distribution can be obtained by this method, using the following Eqs.

(1) and (2) (Hernández *et al.* 1996)

$$(P_h - P_l) \times \pi r^2 = \Delta P \times \pi r^2 = r \cdot 2\pi r \quad (1)$$

$$r = \frac{2\gamma \cdot \cos\theta}{\Delta P} \rightarrow \Delta P = \frac{2\gamma \cdot \cos\theta}{r} \quad (2)$$

where  $r$  is the radius;  $\gamma$  is the surface tension;  $P_l$  is the lowest pressure within the liquid phase; and  $P_h$  is the highest pressure during the gas phase.

Surface porosity and pore density of the composite membranes were studied by a statistic method (Sarbolouki 1982). When membranes are assumed to have asymmetric structures, surface porosity is calculated using the following Eq. (3)

$$\varepsilon = \frac{3\pi\eta J_w}{R \times \Delta P} \quad (3)$$

where  $\varepsilon$  is the surface porosity;  $\eta$  is the viscosity of the permeate (g/cm·s);  $J_w$  is the pure water flux (cm/s);  $R$  is the average pore radius (cm) and  $\Delta P$  is the applied pressure (dyn/cm<sup>2</sup>).

From the values of the above equation, pore density was found by following Eq. (4)

$$n = \frac{\varepsilon}{\pi \times R^2} \quad (4)$$

where  $n$  is number of pores/cm<sup>2</sup>.

### 2.3.4 Contact angle of membrane surface

A contact angle system (Phoenix 300, SEO) was used to measure the static contact angle between liquid and membranes by applying sessile drop method. A water droplet of 20  $\mu$ l was put on membrane surfaces and the shapes of the drop, specifically the contact angle, were measured.

### 2.3.5 Surface roughness

Atomic force microscopy (AFM, Park Systems, XE-BIO, Korea) was used to investigate the surface roughness of the membranes. For AFM measurements, preserved membranes were carefully washed with deionized water, and dried on convection oven at 30°C. Samples (1 cm  $\times$  1 cm) were prepared and placed on slide glasses. The prepared membrane samples were scanned over a specific area (5.0  $\mu$ m  $\times$  5.0  $\mu$ m) by cantilever tapping to determine root average arithmetic roughness (Ra).

### 2.3.6 Pure water flux

Amicon stirred cell (Model 8050, Millipore, USA) has a dead end system fixed at 550 rpm by a stirrer (PC-420, Corning, USA), which was used to measure the pure water flux of membranes. Permeation of pure water through membranes was calculated by the following Eq. (5)

$$J(LMH) = \frac{V}{AT} \quad (5)$$

where  $V$  is the volume of the water permeation (L);  $A$  is the effective membrane area (m<sup>2</sup>); and  $T$  is

the permeation time (h). In this study, the effective membrane area was  $0.00134 \text{ m}^2$  and driving force of 10 psig was maintained with purified nitrogen gas.

### 2.3.7 Particle rejection

Kaolin particles ( $0.1\text{--}4 \mu\text{m}$ ) were added in DI water to prepare a  $60 \pm 5$  NTU (Nephelometric Turbidity Unit) solution of suspended particles to test MF membrane performance. The turbidity of solution was measured using a turbidimeter (model 2100P, Hach, USA).

The membranes were set in a dead-end system using the Amicon cell at 10 psig to investigate particle rejection efficiency of the membranes. Then, the rejection rate was re-measured under the same conditions for 30 min with each process repeated twice. After every step, the turbidity of permeate was checked and compared with that of the feed solution.

### 2.3.8 Fouling test of organic matter

Humic acid powder was dissolved in DI water to produce a 2 ppm humic acid solution. Floating particles in the solution were eliminated with filter paper (No. 5c, Advantec, Japan). A pH meter (8102BNUWP, Thermo Scientific, USA) was used to adjust the solution to  $\text{pH } 7.0 \pm 0.1$  by addition of  $0.1 \text{ M NaOH}$  and  $\text{HCl}$ .

Fouling tests were conducted in the same stirred cell system used for the pure water flux calculations. Pure water was permeated for 120 min to achieve a steady state. Then, humic acid solution was permeated through the membranes to evaluate their fouling resistance. All experiments were performed at room temperature with constant pressure of 10 psig.

## 3. Results and discussion

### 3.1 Element analysis of membrane surface

The composition of  $C_{60}$  and PVDF on the membrane surface was analyzed by element analysis. Various methods have been tried to confirm the existence of particles in membranes, including fourier transform infrared spectroscopy (FT-IR), SEM, and TEM. However, in this study, surface distribution of particles was detected by EDS, taking into account the characteristic of  $C_{60}$ . Fig. 1 shows the atomic rates determined through energy dispersive X-ray spectroscopy (EDS) spectra.  $C_{60}$  nanoparticles are distributed on the surface of PVDF composite membranes despite low composition. As the content of  $C_{60}$  in the composite membrane increases, the carbon content of the surface also increases while the ratio of fluorine decreases.

### 3.2 Hydrophilicity of composite membranes

Hydrophilicity of the composite membrane surfaces was estimated by contact angle measurements. The sessile drop technique (SDT) was used to characterize solid surface energies in measuring membrane surface tension and surface energy. The value of the water contact angle is quantitatively related to the free hydration energies of the membrane (Lapointe *et al.* 2005).

This study also used water contact angle as an indicator of hydrophilicity of membrane surfaces.  $C_{60}$  is known to be a hydrophobic nanoparticle in aqueous systems. Under aqueous conditions,  $C_{60}$  aggregation occurs due to hydrophobic attraction and high cohesion of water.

$C_{60}$  has high free hydration energy ( $\Delta G_{pw}^{\text{total}} = -90.5 \text{ mJ/m}^2$ ), which indicates a high degree of

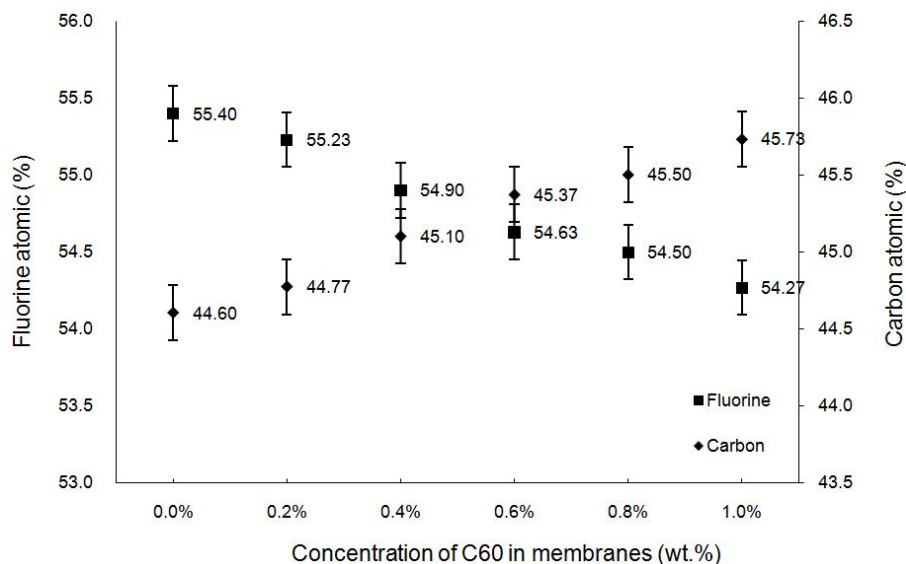


Fig. 1 Composition analysis of membrane surfaces with varying C<sub>60</sub> content

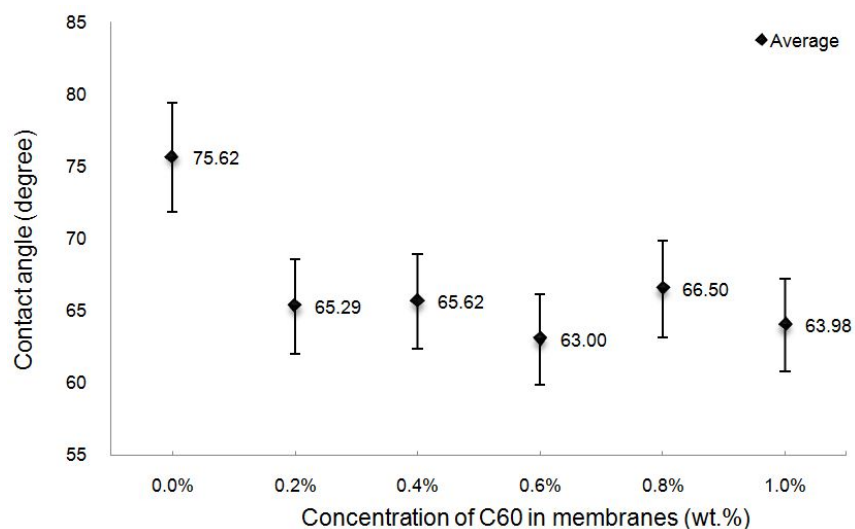


Fig. 2 Changes in static contact angle values for different concentrations of C<sub>60</sub>

affinity for water (Ma *et al.* 2010). Moreover, the contact angle of C<sub>60</sub> is known to be near 60°; this is evidence that C<sub>60</sub> is a hydrophilic additive compared to the 80° contact angle of PVDF polymer (Hong and He 2012).

In cases where C<sub>60</sub> is well-dispersed, the difference in contact angle is an indicator of its affinity for water. Fig. 2 shows that addition of C<sub>60</sub> results in decreases in contact angles. This result is also evidence of even distribution of C<sub>60</sub> on membrane surfaces.

### 3.3 Surface roughness of composite membranes (AFM)

To confirm the surface roughness of the composite membranes, atomic force microscopy (AFM) was used to make a comparison with SEM results. In Fig. 3, the bright part is the highest point of the membrane, while the dark part is a valley or pore. The parameters of the surfaces roughness of the PVDF/ $C_{60}$  membranes are listed in Table 2.

Surface roughness of all composite membranes shows higher value than that of the pristine membranes. The  $C_{60}$ -3 membrane has the highest value (Ra. 67.25), which means that it has the roughest surface (with the greatest number of pores) and the widest active layer surface among composite membranes; this also explains its relatively high flux value as shown in Fig. 8.

### 3.4 Pore size and distribution

Table 3 shows the characterization of membrane pores. The average pore size of pristine PVDF membranes is  $0.22 \mu\text{m}$  and the bubble point (BP), which refers to maximum pore size, is  $2.27 \mu\text{m}$ , approximately 10 times bigger than the average pore size. Adding the  $C_{60}$  slightly decreases pore size, presumably due to the interaction between  $C_{60}$  and PVDF during the structure formation process. As a result, bubble point also shows an overall decrease in size.

The composite membranes in this study exhibited uniform porous characteristics. The pore size distribution of membrane  $C_{60}$ -0 and membrane  $C_{60}$ -3 are shown in Figs. 4 and 5 respectively. The sharp peak of the graph is greatly focused on mean pore size, and shifts to the left with the

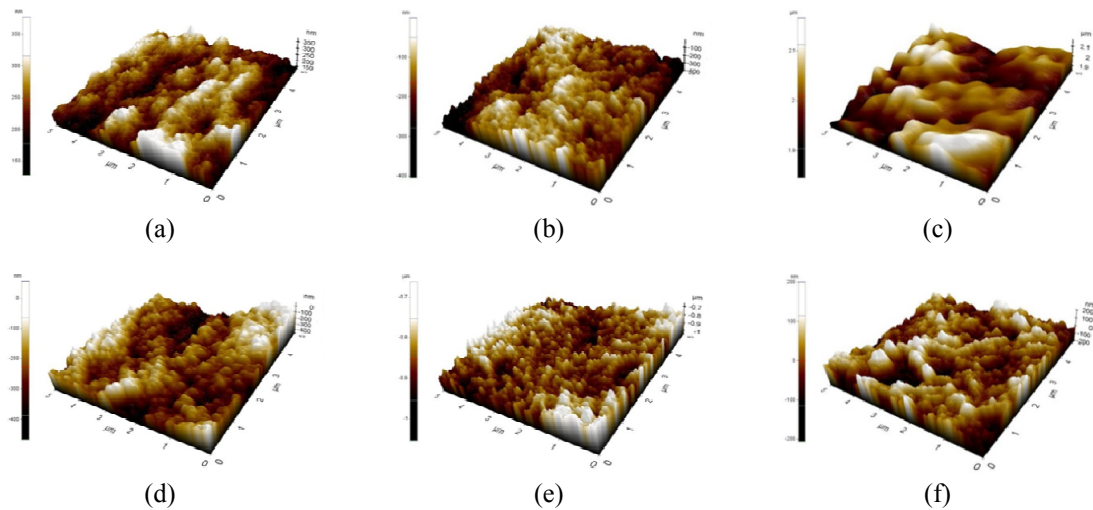


Fig. 3 Three-dimensional AFM images of the membranes: (a)  $C_{60}$ -0; (b)  $C_{60}$ -1; (c)  $C_{60}$ -2; (d)  $C_{60}$ -3; (e)  $C_{60}$ -4; (f)  $C_{60}$ -5

Table 2 Surface roughness of composite membranes

Composite membrane	$C_{60}$ -0	$C_{60}$ -1	$C_{60}$ -2	$C_{60}$ -3	$C_{60}$ -4	$C_{60}$ -5
$R_a$ (nm)	33.02	44.42	42.83	67.25	39.77	46.11

Table 3 Pore properties on membrane surfaces

Pore size	Membrane	C <sub>60</sub> -0	C <sub>60</sub> -1	C <sub>60</sub> -2	C <sub>60</sub> -3	C <sub>60</sub> -4	C <sub>60</sub> -5
Average pore diameter ( $\mu\text{m}$ )		0.220	0.200	0.208	0.206	0.218	0.209
Bubble point pore diameter ( $\mu\text{m}$ )		2.271	1.290	1.856	2.142	1.612	1.285

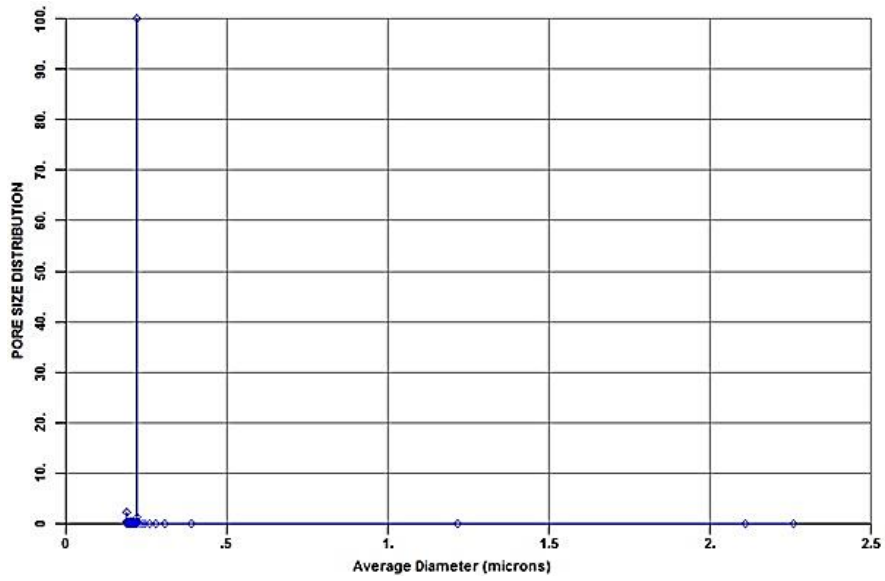


Fig. 4 Pore size distribution of C<sub>60</sub>-0

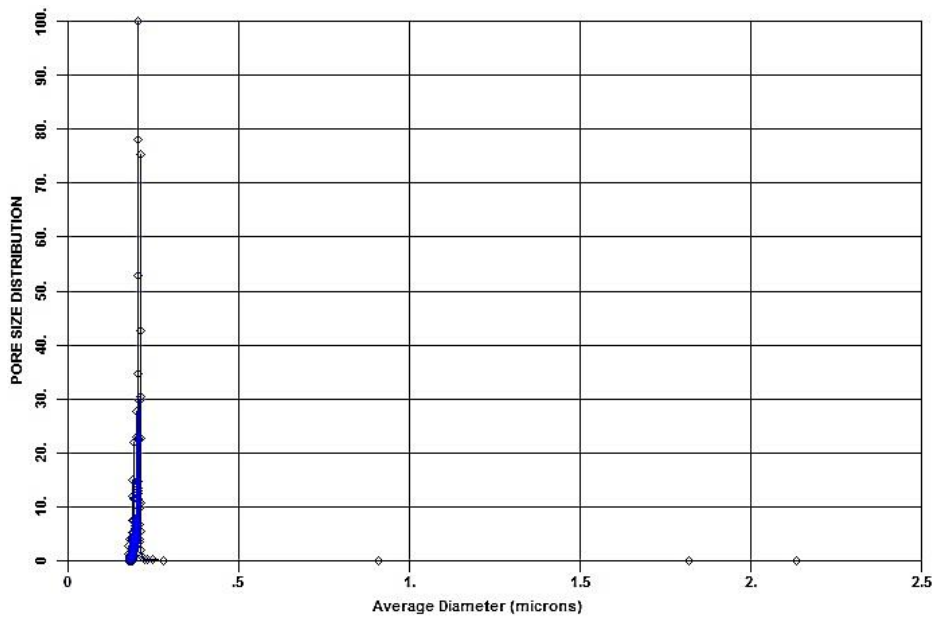


Fig. 5 Pore size distribution of C<sub>60</sub>-3

addition of particles.

The pore size of the  $C_{60}$ -embedded membranes is about 10% smaller compared with pristine PVDF membranes, and their bubble point pore diameter is also smaller relative to those of pristine PVDF membranes.

### 3.5 Membrane morphology

In order to investigate the effect of  $C_{60}$  nanoparticles on the morphology of the membranes, the surface and cross-section images of PVDF membranes were obtained by SEM. Fig. 6 shows the membrane surfaces magnified at 20,000x. Both the pristine and composite membranes show numerous pores on their surfaces. This indicates that all membranes have pores on their surfaces and uniform pore sizes despite presence of increased particles in the composite membranes.

Fig. 7 shows the morphology of cross-sections magnified at 500x. Pure PVDF membranes exhibit asymmetric structure from top to bottom, dense active layer, porous finger-like structures, and cellular porous walls. All composite membranes with varying  $C_{60}$  concentrations similarly exhibit asymmetric structures.

It is difficult to detect large differences on the surface using SEM photography, because only a small portion of all the membranes were observed. However, more precise surface properties could be determined by using Eqs. (3)-(4). Table 4 lists the surface porosity and pore density of the fabricated membranes. It shows that the  $C_{60}$ -3 membrane has the greatest number of pores. This leads to an increase in effective surface area due to increase in roughness as shown in Table 2, as a direct result of such an increase (Arthanareeswaran *et al.* 2008).

The increase in pore density with the increase of  $C_{60}$  added in his experiment can be explained by the polymer- $C_{60}$  interfacial surface area between the polymer,  $C_{60}$ , and solvent, and changes in the demixing rate due to the affinity of the dope solution to polar non-solvents. Previous studies have shown that addition of porogens such as PVP increase thermodynamic instability which stimulates demixing in dope solution (Taurozzi *et al.* 2011). Julian S. Taurozzi explained that hydrophobicity also had a similar effect to that of porogen in the demixing process of  $C_{60}$ , which was attributable to the hydrophobicity of  $C_{60}$ . In other words, as the amount of  $C_{60}$  increases, phase separation and demixing is accelerated due to the overall decrease in affinity of casting mixture to polar non-solvent (water). The demixing rate is related to the amount of  $C_{60}$  added and the resulting surface area of the particle. The affinity of the casting mixture to the polar non-solvent (water) decreases as the surface area of the hydrophobic  $C_{60}$  increases. However, the surface area of  $C_{60}$  does not continue to increase. As the amount of  $C_{60}$  added increases, the surface area increases initially due to distribution, but above a certain concentration level, aggregation of accumulated  $C_{60}$  occurs due to an increase in the frequency of particle collisions and enthalpic interaction between solvent and  $C_{60}$ , which results in a decrease in particle surface area. Julian S. Taurozzi also explained through experiments that the effect of  $C_{60}$  surface area on demixing rate is greater at nanoscale particle sizes, but minimal at macroscale sizes. Accordingly, the increase in demixing rate due to increase in amount of  $C_{60}$  added is not continuous, but attains an optimized value at some point.

In general, porous membranes are made at higher demixing rates. It may be predicted that membranes of the highest pore density can be made in dope solution containing amount of  $C_{60}$  which resulting in optimized demixing rate. In this study, for the above reasons, the  $C_{60}$ -3 ( $C_{60}$ /PVDF(%): 0.6%) membrane, which displayed the highest pore density, may be presumed to display the highest demixing rate during fabrication.

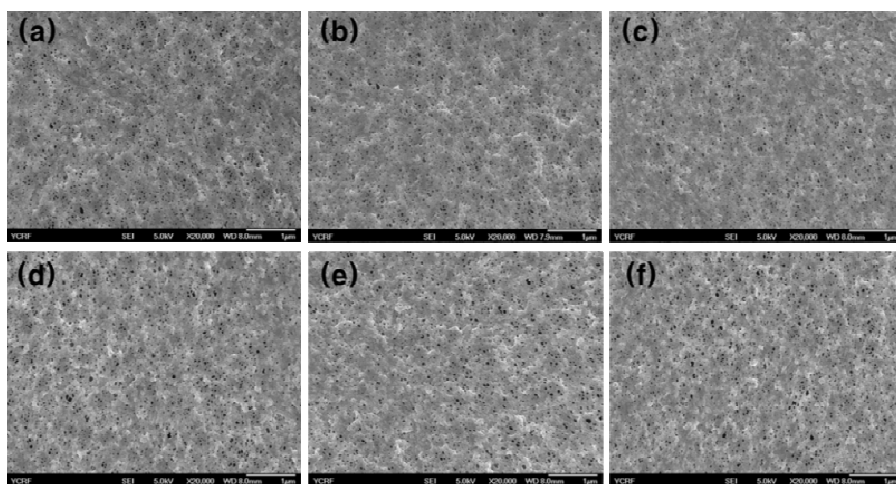


Fig. 6 SEM surface micrographs of the membranes: (a) C<sub>60</sub>-0; (b) C<sub>60</sub>-1; (c) C<sub>60</sub>-2; (d) C<sub>60</sub>-3; (e) C<sub>60</sub>-4; (f) C<sub>60</sub>-5

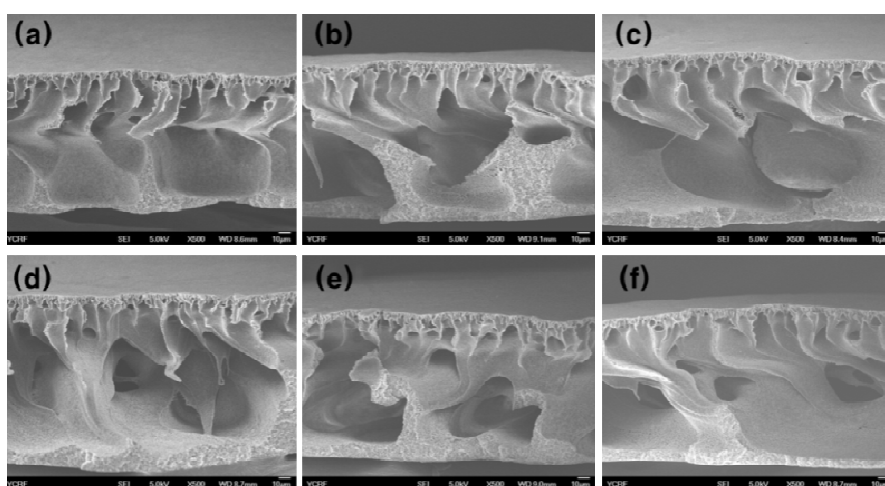


Fig. 7 SEM cross-sectional micrographs of the membranes: (a) C<sub>60</sub>-0; (b) C<sub>60</sub>-1; (c) C<sub>60</sub>-2; (d) C<sub>60</sub>-3; (e) C<sub>60</sub>-4; (f) C<sub>60</sub>-5

Table 4 Surface porosity and pore density of composite membranes

Composite membrane	Surface porosity ( $\times 10^{-5}$ )	Pore density (pores/cm <sup>2</sup> )
C <sub>60</sub> -0	11.04	72633
C <sub>60</sub> -1	13.63	108422
C <sub>60</sub> -2	13.38	98427
C <sub>60</sub> -3	15.35	115161
C <sub>60</sub> -4	12.16	81428
C <sub>60</sub> -5	12.00	87437

Table 5 Mechanical strength of composite membranes

Composite membrane	Elongation at break (%)	Tensile strength (kPa)
$C_{60}$ -0	40.50	752.62
$C_{60}$ -1	40.49	753.35
$C_{60}$ -2	40.49	730.97
$C_{60}$ -3	40.50	711.04
$C_{60}$ -4	40.49	742.81
$C_{60}$ -5	40.50	750.54

### 3.6 Mechanical strength of membranes

Table 5 shows the elongation at break and tensile strength of the polymeric membranes containing  $C_{60}$ , compared to that of the pristine membrane. All supportless composite membranes have about 40.5% of elongation at break when the tensile strength is around 710-750 kPa. In general, membrane porosity is higher at faster demixing rates, and tensile strength is lower at higher membrane porosities (Biesheuvel and Verweij 1999, Hsieh 1996, Qin and Chung 1999), and this experiment results also showed tendencies similar to this general phenomenon. However, the relationship between membrane porosity and tensile strength is not always so consistent. It may be presumed that there are other factors involved, such as optimization of interaction between  $C_{60}$  and polymer.

### 3.7 Pure water flux

In general, multiple factors including surface pore size, cross-section morphology, and hydrophilicity determine membrane flux (Li *et al.* 2009). As the cross-section morphologies were similar for the pristine membrane and composite membranes, interpretation of study results was focused on other factors, i.e., pore size and hydrophilicity.

The flux results of this study are quite remarkable. Fig. 8 shows the average pure water flux of each membrane at steady state (after 120 minutes). The addition of  $C_{60}$  has an effect on pure water permeation flux. In particular, the flux for the  $C_{60}$ -3 (931 LMH) membrane is about 30% higher than the  $C_{60}$ -0 (715 LMH) membrane. Also, the flux shows a similar pattern to surface roughness. The  $C_{60}$ -3 membrane, which had the roughest surface, also has the most effective flux.

In addition, the difference in the rate of pore size reduction between the  $C_{60}$ -0 membrane and the  $C_{60}$ -3 membrane is approximately 10 percent (Table 3). Based on Eq. (6), which shows the relation between flux and pore size, the flux of the  $C_{60}$ -3 membrane should be around 60 percent of that of the  $C_{60}$ -0 membrane. However, the actual result was almost 90 percent; this result can be explained by the affinity of  $C_{60}$  particles for water, acting as a hydrophilic additive which increases water permeation flux. In addition, the increase in the number of pores as shown in Table 4 led to an increase in the amount of water passing through the membranes.

$$J \propto r^4 \tag{5}$$

### 3.8 Fouling test of organic matter

Organic fouling resistance was measured by filtration of humic acid solution through a

dead-end system at steady state (after 120 minutes). In general, under comparable pore size conditions, the degree of fouling declines at higher levels of hydrophilicity. However, Table 6 shows that the C<sub>60</sub>-3 membrane, which has the highest level of hydrophilicity (63.00°), exhibits the worst fouling (0.26) among all the samples. These study results can be explained by the differences in flux performance for each membrane, as C<sub>60</sub>-3 had more fouling feed permeate the membrane due to its higher flux (932LMH) than other membranes. Relatively faster feed solution permeation leads to more severe fouling due to greater humic acid adsorption and more rapid cake layer formation (Marshall *et al.* 1997). The pure water flux tendencies in Fig. 8 show results which are opposite to the fouling test results in Table 6, confirming that fouling is dependent on flux at comparable pore size and hydrophilicity conditions. In addition, lower surface roughness is known to result in higher antifouling ability (Rana and Matsuura 2010). shows the smallest decline in flux for the pristine PVDF membrane, which has smooth surface. The increased surface roughness with the addition of particles also contributes to decrease in fouling resistance (Oh *et al.* 2009).

### 3.9 Particle rejection test

The rejection efficiency of MF membranes was calculated by the reduction of Kaolin concentration in the feed solution. The pristine PVDF membrane and the high-performance embedded membrane (C<sub>60</sub>-3) were selected for the rejection test for comparison purposes. The initial turbidity of feed solution was 60 NTU, and the pristine PVDF and PVDF/C<sub>60</sub> membranes removed about 99.5% of suspended particles. The turbidity of permeate is shown in Table 7. The C<sub>60</sub>-3 membrane shows better performance than the pristine membrane after the back washing process. Its higher roughness compared to that of the pristine membrane may reduce adhesion of

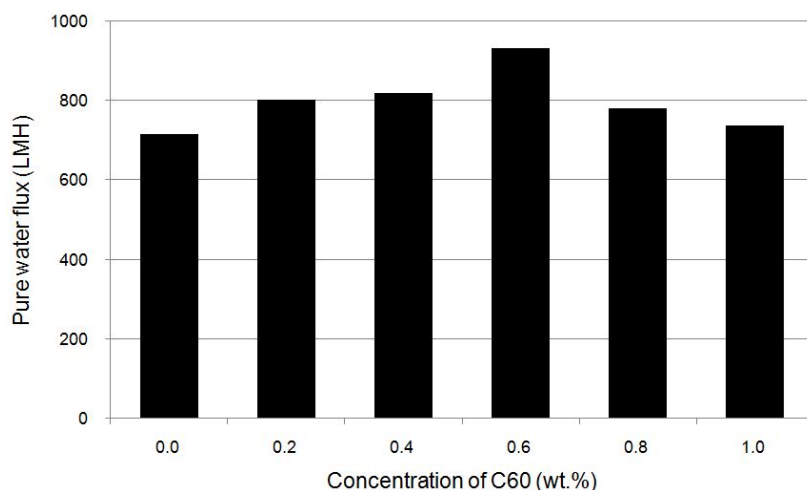


Fig. 8 Pure water flux of fullerene-blended PVDF composite membranes at steady state

Table 6 Normalized filtrate flux of 2 ppm humic acid solution at steady state

Concentration of C <sub>60</sub> (wt.%)	C <sub>60</sub> -0	C <sub>60</sub> -1	C <sub>60</sub> -2	C <sub>60</sub> -3	C <sub>60</sub> -4	C <sub>60</sub> -5
Normalized flux (J/J <sub>0</sub> )	0.34	0.31	0.27	0.26	0.28	0.31

Table 7 Turbidity of permeate

Composite membrane (Turbidity)	Time (min)			
	0	60	90	120
$C_{60}$ -0 (NTU)	60	0.26	0.35	0.45
$C_{60}$ -3 (NTU)	60	0.30	0.35	0.42

suspended particles. Table 2 shows that  $C_{60}$ -3 has the roughest surface, and the gap of the rejection rate may be attributed to this roughness (Hashino *et al.* 2011).

#### 4. Conclusions

In this study, PVDF MF membranes and PVDF/ $C_{60}$  composite membranes were fabricated by non-solvent induced phase separation method. Their characteristics were investigated using various techniques. The results show that the addition of  $C_{60}$  particles does not cause fraction and the composite membranes have stable morphology on their surfaces and cross-sections. The addition of  $C_{60}$  results in an improvement of hydrophilicity in composite membranes. Despite smaller pore sizes, PVDF/ $C_{60}$  composite membranes have higher flux than pristine PVDF membranes because of remarkable surface porosity and pore density, as well as high surface roughness. On the other hand, this porosity resulted in a marginal weakening of tensile strength, but also brought about considerable increases in flux. Fouling tests show that PVDF/ $C_{60}$  composite membranes have higher fouling than pristine PVDF membranes, which is the result of greater feed solution flow through the membrane over an extended period of time. This result also helps to explain the increase in flux of the PVDF/ $C_{60}$  composite membranes due to increase in number of pores. Moreover, it was proven through particle rejection tests that the fabricated membranes could function as MF.

A 0.6 wt.% concentration of  $C_{60}$  by weight in the casting solution produced the most optimal properties among the composite membranes tested. As  $C_{60}$  is very expensive, it is especially worth noting that the addition of even a small amount of  $C_{60}$  can produce significant improvement.

#### Acknowledgments

This work was supported by a grant (No. 2103-11-1437) from the Yang Young Foundation, funded by Samyang Corporation.

#### References

- Arthanareeswaran, G., Sriyamuna Devi, T. and Raajenthiren, M. (2008), "Effect of silica particles on cellulose acetate blend ultrafiltration membranes: Part I", *Sep. Purif. Technol.*, **64**(1), 38-47.
- Bae, T.-H. and Tak, T.-M. (2005), "Effect of  $TiO_2$  nanoparticles on fouling mitigation of ultrafiltration membranes for activated sludge filtration", *J. Membr. Sci.*, **249**(1-2), 1-8.
- Biesheuvel, P.M. and Verweij, H. (1999), "Design of ceramic membrane supports: permeability, tensile strength and stress", *J. Membr. Sci.*, **156**(1), 141-152.

- Bottino, A., Capannelli, G. and Comite, A. (2005), "Novel porous poly (vinylidene fluoride) membranes for membrane distillation", *Desalination*, **183**(1), 375-382.
- Cao, X., Ma, J., Shi, X. and Ren, Z. (2006), "Effect of TiO<sub>2</sub> nanoparticle size on the performance of PVDF membrane", *Appl. Surf. Sci.*, **253**(4), 2003-2010.
- Chae, S.-R., Yamamura, H., Ikeda, K. and Watanabe, Y. (2008), "Comparison of fouling characteristics of two different poly-vinylidene fluoride microfiltration membranes in a pilot-scale drinking water treatment system using pre-coagulation/sedimentation, sand filtration, and chlorination", *Water Res.*, **42**(8), 2029-2042.
- Hashino, M., Katagiri, T., Kubota, N., Ohmukai, Y., Maruyama, T. and Matsuyama, H. (2011), "Effect of surface roughness of hollow fiber membranes with gear-shaped structure on membrane fouling by sodium alginate", *J. Membr. Sci.*, **366**(1), 389-397.
- Hernández, A., Calvo, J., Prádanos, P. and Tejerina, F. (1996), "Pore size distributions in microporous membranes. A critical analysis of the bubble point extended method", *J. Membr. Sci.*, **112**(1), 1-12.
- Hong, J. and He, Y. (2012), "Effects of nano sized zinc oxide on the performance of PVDF microfiltration membranes", *Desalination*, **302**(0), 71-79.
- Hsieh, H. (1996), *Inorganic Membranes for Separation and Reaction*, Elsevier.
- Lapointe, J.-F., Gauthier, S.F., Pouliot, Y. and Bouchard, C. (2005), "Characterization of interactions between  $\beta$ -lactoglobulin tryptic peptides and a nanofiltration membrane: Impact on the surface membrane properties as determined by contact angle measurements", *J. Membr. Sci.*, **261**(1), 36-48.
- Li, J.-F., Xu, Z.-L., Yang, H., Yu, L.-Y. and Liu, M. (2009), "Effect of TiO<sub>2</sub> nanoparticles on the surface morphology and performance of microporous PES membrane", *Appl. Surf. Sci.*, **255**(9), 4725-4732.
- Ma, X., Wigington, B. and Bouchard, D. (2010), "Fullerene C60: Surface Energy and Interfacial Interactions in Aqueous Systems", *Langmuir*, **26**(14), 11886-11893.
- Madaeni, S.S. and Yeganeh, M.K. (2003), "Microfiltration of emulsified oil wastewater", *J. Porous Mater.*, **10**(2), 131-138.
- Marshall, A., Munro, P. and Trägårdh, G. (1997), "Influence of permeate flux on fouling during the microfiltration of  $\beta$ -lactoglobulin solutions under cross-flow conditions", *J. Membr. Sci.*, **130**(1), 23-30.
- Ochoa, N., Masuelli, M. and Marchese, J. (2003), "Effect of hydrophilicity on fouling of an emulsified oil wastewater with PVDF/PMMA membranes", *J. Membr. Sci.*, **226**(1), 203-211.
- Oh, S.J., Kim, N. and Lee, Y.T. (2009), "Preparation and characterization of PVDF/TiO<sub>2</sub> organic-inorganic composite membranes for fouling resistance improvement", *J. Membr. Sci.*, **345**(1), 13-20.
- Oshima, K., Evans-Strickfaden, T., Highsmith, A. and Ades, E. (1996), "The use of a microporous polyvinylidene fluoride (PVDF) membrane filter to separate contaminating viral particles from biologically important proteins", *Biologicals*, **24**(2), 137-145.
- Park, H.-H., Lim, C.-W., Jo, H.-D., Choi, W.-K. and Lee, H.-K. (2007), "Absorption of SO<sub>2</sub> using PVDF hollow fiber membranes with PEG as an additive", *Korean J. Chem. Eng.*, **24**(4), 693-697.
- Qin, J. and Chung, T.-S. (1999), "Effect of dope flow rate on the morphology, separation performance, thermal and mechanical properties of ultrafiltration hollow fibre membranes", *J. Membr. Sci.*, **157**(1), 35-51.
- Rahimpour, A., Jahanshahi, M., Rajaeian, B. and Rahimnejad, M. (2011), "TiO<sub>2</sub> entrapped nano-composite PVDF/SPES membranes: Preparation, characterization, antifouling and antibacterial properties", *Desalination*, **278**(1), 343-353.
- Rana, D. and Matsuura, T. (2010), "Surface modifications for antifouling membranes", *Chem. Rev.*, **110**(4), 2448-2471.
- Sarbolouki, M. (1982), "A general diagram for estimating pore size of ultrafiltration and reverse osmosis membranes", *Sep. Sci. Technol.*, **17**(2), 381-386.
- Tan, X., Tan, S., Teo, W. and Li, K. (2006), "Polyvinylidene fluoride (PVDF) hollow fibre membranes for ammonia removal from water", *J. Membr. Sci.*, **271**(1), 59-68.
- Taurozzi, J.S., Crock, C.A. and Tarabara, V.V. (2011), "C60-polysulfone nanocomposite membranes: Entropic and enthalpic determinants of C60 aggregation and its effects on membrane properties", *Desalination*, **269**(1), 111-119.

- Vatanpour, V., Madaeni, S.S., Moradian, R., Zinadini, S. and Astinchap, B. (2011), "Fabrication and characterization of novel antifouling nanofiltration membrane prepared from oxidized multiwalled carbon nanotube/polyethersulfone nanocomposite", *J. Membr. Sci.*, **375**(1), 284-294.
- Wang, P., Tan, K., Kang, E. and Neoh, K. (2002), "Plasma-induced immobilization of poly (ethylene glycol) onto poly (vinylidene fluoride) microporous membrane", *J. Membr. Sci.*, **195**(1), 103-114.
- Wang, D., Teo, W. and Li, K. (2004), "Selective removal of trace H<sub>2</sub>S from gas streams containing CO<sub>2</sub> using hollow fibre membrane modules/contractors", *Sep. Purif. Technol.*, **35**(2), 125-131.
- Wu, G., Gan, S., Cui, L. and Xu, Y. (2008), "Preparation and characterization of PES/TiO<sub>2</sub> composite membranes", *Appl. Surf. Sci.*, **254**(21), 7080-7086.
- Yan, L., Li, Y.S., Xiang, C.B. and Xianda, S. (2006), "Effect of nano-sized Al<sub>2</sub>O<sub>3</sub>-particle addition on PVDF ultrafiltration membrane performance", *J. Membr. Sci.*, **276**(12), 162-167.
- Yang, X., Deng, B., Liu, Z., Shi, L., Bian, X., Yu, M., Li, L., Li, J. and Lu, X. (2010), "Microfiltration membranes prepared from acryl amide grafted poly (vinylidene fluoride) powder and their pH sensitive behaviour", *J. Membr. Sci.*, **362**(1), 298-305.
- Zhang, M., Nguyen, Q.T. and Ping, Z. (2009), "Hydrophilic modification of poly (vinylidene fluoride) microporous membrane", *J. Membr. Sci.*, **327**(1-2), 78-86.
- Zheng, Y.-M., Zou, S.-W., Nanayakkara, K.G.N., Matsuura, T. and Chen, J.P. (2011), "Adsorptive removal of arsenic from aqueous solution by a PVDF/zirconia blend flat sheet membrane", *J. Membr. Sci.*, **374**(1-2), 1-11.